AIAA SciTech Forum
11–15 & 19–21 January 2021, VIRTUAL EVENT
AIAA Scitech 2021 Forum

10.2514/6.2021-1141

Toward Numerical Investigation of Ignition and Combustion Transition in a Subscale LOX/Methane Rocket Combustor

Matthew Bonanni*, Danyal Mohaddes†, and Nguyen Ly‡
Stanford University, Stanford, CA, 94305

Nikolaos Perakis§
Technical University of Munich, Garching, 85748, Germany

Justin Hardi¶ and Michael Börner‖
German Aerospace Center (DLR), Hardthausen, 74239, Germany

Matthias Ihme**
Stanford University, Stanford, CA, 94305

LOX/methane is a promising alternative to hypergolic fuels in spacecraft thrusters, featuring advantages such as nontoxicity, high specific impulse, and low cost. Its reliable ignition, however, is a challenging problem due to its dependence on the local mixture composition, its requirement of overcoming ionization energies, and its process of transition to a sustained combustion mode. Experimental research has focused on laser pulses as an ignition mechanism for these thrusters, and has demonstrated significant viability. This work presents a numerical study of a reacting LOX/methane thruster using large eddy simulation combined with a Lagrangian description of the LOX spray. This model is successfully employed to simulate reacting flow in the Reaction Control System (RCS) breadboard combustor at DLR, achieving spray behavior that is qualitatively similar to the pre-ignition experimental data. This work represents a forward step towards simulating the startup process of this thruster via laser ignition.

*Graduate student, Mechanical Engineering, mbonanni@stanford.edu
†Graduate student, Mechanical Engineering
‡Graduate student, Mechanical Engineering
§Graduate student, Chair of Space Propulsion
¶Leader Combustion Dynamics, Institute of Space Propulsion
‖Research and Test Engineer, Institute of Space Propulsion
**Associate Professor, Mechanical Engineering

I. Nomenclature

c	=	heat capacity	Sc	=	Schmidt number
C	=	progress variable	Sh	=	Sherwood number
D_l	=	LOX inlet diameter	$\boldsymbol{u}$	=	velocity
H_M	=	mass transfer potential	We	=	Weber number
j	=	species flux	Y_k	=	species mass fraction of the k-th species
J	=	momentum flux ratio	Z	=	mixture fraction
L	=	LOX cone length	θ	=	axial spray injection angle
m_d	=	droplet mass	μ	=	dynamic viscosity
Nu	=	Nusselt number	ρ	=	density
p	=	pressure	σ	=	surface tension
Pr	=	Prandtl number	τ	=	viscous stress tensor
$\boldsymbol{q}$	=	heat flux	τ_x	=	characteristic time associated with x
Re	=	Reynolds number	$\dot{\omega}$	=	reaction source term

II. Introduction

Traditionally, chemical thrusters for spacecraft have used hypergolic propellants, commonly dinitrogen tetroxide (NTO) and variants of hydrazine [1]. This is largely because of their reliability – their hypergolicity ensures ignition with no need for an external energy source. Nonhypergolic propellants, however, are of increasing interest in recent years due to some critical advantages. Chief among these is their ease of handling, in comparison to the high toxicity and material incompatibilities of hypergolic fuels. Among the candidate alternative propellants, the combination of liquid oxygen and gaseous methane is a promising one, as it combines a high specific impulse with low cost and high sustainability. Moreover, methane is also particularly attractive for use in future space vehicles taking advantage of in-situ resource utilization, as it may be synthesized on the surface of the Mars or other planetary bodies by taking advantage of the Sabatier process [2]. Compared to the combination of hydrogen/oxygen, methane has the advantage of a greater volumetric density, leading to lower structural mass, [3] and a higher boiling temperature, which simplifies the thermal control of the spacecraft and enables a longer fatigue life expectancy [4].

The ignition and stable combustion of LOX/methane, however, is a significant engineering challenge. Common approaches to ignition in primary stage engines include secondary hypergolic fuel systems and electric sparks. Laser ignition features advantages such as improved precision in both ignition location and time as well as increased flexibility in propellant and environmental conditions [5]. This approach has been experimentally studied at the DLR Institute of Space Propulsion using the Reaction Control System (RCS) breadboard combustor at the M3.1 test bench in two configurations: laser ablation of a metal target and direct plasma ignition. The ignition process has also been characterized in a numerical study of its predecessor, the microcombustor of the M3 test bench, using gaseous methane and oxygen as propellants [6]. The goal of this work is to numerically model the Manfletti 2014 gaseous methane liquid oxygen case, using large eddy simulation (LES) in conjunction with a Lagrangian spray model to describe the liquid oxygen injection and phase transition by heat transfer and flash evaporation. As a step towards this goal, we present a simulation of combustion in this device. We also present the formulation of a model for simulating its full ignition process in the future, using finite rate chemistry with a Gaussian energy deposition model for the laser ignition.

III. Reference Experiment

The RCS breadboard combustor is an experimental thruster with windows for optical measurement and laser access. In the Manfletti 2014 configuration, a shear-coaxial injector is installed, with gaseous methane injected in an annulus surrounding the LOX core. The parameters of this injector are summarized in Table 1, yielding a rich oxygen-fuel ratio of 3.17. Prior to startup, a vacuum pump reduces the chamber pressure to approximately 20-75 mbar. Subsequently, LOX is injected to chill the chamber for a period of 200 ms. The ignition process then begins with either fuel or LOX preflow, and, some time after the other propellant flow begins, the laser pulse is fired to trigger ignition. The chamber pressure is approximately 200 mbar at this time for the GCH4 case, and rises to 1.5-1.7 bar after steady state combustion is reached. Note that the GCH4 flow is significantly underexpanded, and the listed properties represent the state at the fuel dome.

Table 1 Injection Conditions [5]

	GCH4	LOX
Mass flow rate (g/s)	18	57
Dome pressure (Pa)	12.5×10^5	2.5×10^5
Temperature (K)	205	90
Injector ID (mm)	3.2	~
Injector OD (mm)	5	2.4

Rather than modeling the entire startup sequence from the moment the propellants start to flow, the ignition simulation will first verify that the flow has reached a non-reacting steady state by the time the laser pulse occurs. The combustion model will then be applied as the ignition is triggered from this steady state injection condition, in order to capture the flame evolution. This simplification is justified by the following analysis: we may approximate a time scale associated with the LOX flow along the length of the core as

$$\tau_{\text{core}} = \frac{L}{u_l}, \tag{1}$$

where L is the length of the LOX cone (described in greater detail in Sec. V) and u_l is the LOX feed velocity. For this case, $\tau_{\text{core}} \approx 1.25$ ms. In comparison, τ_{ig}, the time between full propellant flow and ignition, is no less than 75 ms [5]. Therefore, the ratio of these time scales

$$\frac{\tau_{\text{ig}}}{\tau_{\text{core}}} \approx 60$$

demonstrates that the flow can safely be assumed to have reached steady state by the time ignition is triggered.

IV. Mathematical Formulation

A. Gas-phase equations

The model to be used in this work combines the standard Eulerian LES equations with a Lagrangian model for the spray phase. Details of this formulation are described in [7]. The coupling

from the spray phase appears as additional source terms in the LES equations, yielding

$$D_t\bar{\rho} = -\bar{\rho}\nabla\cdot\tilde{\boldsymbol{u}} + \bar{\dot{S}}_\rho \tag{2a}$$

$$\bar{\rho}D_t\tilde{\boldsymbol{u}} = -\nabla\bar{p} + \nabla\cdot\bar{\boldsymbol{\tau}}_{\nu+t} + \bar{\dot{\boldsymbol{S}}}_{\boldsymbol{u}} \tag{2b}$$

$$\bar{\rho}D_t\tilde{e}_t = -\nabla\cdot(\bar{p}\tilde{\boldsymbol{u}}) + \nabla\cdot(\bar{\boldsymbol{\tau}}_{\nu+t}\cdot\tilde{\boldsymbol{u}}) - \nabla\cdot\bar{\boldsymbol{q}}_{\nu+t} + \bar{\dot{S}}_{e_t} \tag{2c}$$

$$\bar{\rho}D_t\tilde{Y}_k = -\nabla\cdot\bar{\boldsymbol{j}}_{k,\nu+t} + \bar{\dot{\omega}}_k + \bar{\dot{S}}_{Y_k} \tag{2d}$$

where $D_t = \partial_t + \tilde{\boldsymbol{u}}\cdot\nabla$ is the material derivative, and $\boldsymbol{u}$, ρ, p, and $\boldsymbol{\tau}$ are the velocity vector, density, pressure, and viscous stress tensor, respectively. $\boldsymbol{q}$ is the heat flux and e_t is the specific total energy. Y_k, $\boldsymbol{j}_k$, and $\dot{\omega}_k$ are the species mass fraction, species flux, and reaction source term, respectively, for the k-th species, and subscripts ν and t correspond to viscous and turbulent contributions. The $\dot{S}$ terms are sources from the spray phase. The large droplet mass loading in the configuration considered results in reduced numerical stability. In the present simulation, only the source terms in the mass and species equations were activated, leaving the particles effectively one-way coupled in momentum and energy. Activating source terms in all conservation equations while maintaining numerical stability remains a goal of the future work.

The Vreman model [8] is used for subgrid-scale turbulence, and the dynamic thickened-flame model [9] is applied to interactions between the flame and the turbulence. As the both the methane and liquid oxygen in this system are subcritical with respect to pressure, the ideal gas equation of state is used to close the system.

B. Lagrangian spray particle approach

The behavior of spray droplets in the flow field is governed by Lagrangian equations [10]:

$$d_t\boldsymbol{x}_d = \boldsymbol{u}_d, \tag{3a}$$

$$d_t\boldsymbol{u}_d = \frac{f_1}{\tau_d}\left(\tilde{\boldsymbol{u}}\left(\boldsymbol{x}_d\right) - \boldsymbol{u}_d\right), \tag{3b}$$

$$d_tT_d = \frac{\mathrm{Nu}}{3\mathrm{Pr}_g}\frac{c_p}{c_l}\frac{f_2}{\tau_d}\left(\tilde{T}\left(\boldsymbol{x}_d\right) - T_d\right) + \frac{L_v}{c_l}\frac{\dot{m}_d}{m_d}, \tag{3c}$$

$$d_tm_d \equiv \dot{m}_d = -\frac{\mathrm{Sh}}{3\mathrm{Sc}_g}\frac{m_d}{\tau_d}H_M, \tag{3d}$$

where $\boldsymbol{x}_d$, $\boldsymbol{u}_d$, are the droplet position and velocity vectors, and T_d, m_d and $\dot{m}_d$ are the droplet temperature, mass, and mass evaporation rate, respectively. τ_d, the droplet relaxation time, is defined as

$$\tau_d \equiv \frac{\rho_l D_d^2}{18\mu_g} \tag{4}$$

where ρ_l is the liquid density, D_d is the droplet diameter, and μ_g is the dynamic viscosity of the surrounding gas phase. The gas and spray phases are coupled by $\tilde{T}\left(\boldsymbol{x}_d\right)$ and $\tilde{\boldsymbol{u}}\left(\boldsymbol{x}_d\right)$, the gas-phase temperature and velocity. Pr_g, Sc_g, and c_p are the Prandtl number, Schmidt number, and specific heat capacity of the gas phase, and c_l and L_v are the heat capacity and heat of vaporization of the spray phase. Nu and Sh are the droplet Nusselt and Sherwood numbers as defined by [11], and f_1 is a Stokes drag correction [10]. Model M7 from [10] is used to close f_2, the evaporative heat transfer

correction, and H_M, the mass transfer potential. Additional considerations and adjustments related to using LSP in conjunction with the dynamic thickened flame model are described in [7].

As the LOX spray is also significantly superheated during injection, flash evaporation is another important consideration in the ignition process of this system. In the final simulation, a droplet flash evaporation model based on heterogeneous nucleation will be implemented as an additional mass evaporation rate source term in the LSP equations.

C. Finite rate chemistry

In the full ignition simulation, the GRI-Mech 3.0 methane mechanism [12] will be used for finite rate chemistry, with simplification by removing the species and reactions associated with nitrogen and argon, as they do not appear in this system. This yields a mechanism with 34 species and 215 reactions.

D. FPV model

In the present simulation, the flamelet-progress variable (FPV) model formulation [13] was used to model combustion chemistry, whereby instead of solving Eq. (2d) for each species in the chemical mechanism, transport equations are only solved for the mixture fraction $\tilde{Z}$ and non-normalized progress variable $\tilde{C}$:

$$\bar{\rho} D_t \tilde{Z} = -\nabla \cdot \bar{\boldsymbol{j}}_{Z,\nu+t} + \bar{\dot{S}}_Z \tag{5a}$$

$$\bar{\rho} D_t \tilde{C} = -\nabla \cdot \bar{\boldsymbol{j}}_{C,\nu+t} + \bar{\omega}_C \tag{5b}$$

All other scalar quantities are mapped onto a table of $\tilde{Z}$ and $\tilde{C}$, which was generated with one-dimensional simulations of a counterflow diffusion flame using FlameMaster [14] and the GRI-Mech 3.0 methane mechanism [12]. The progress variable was defined as $C = Y_{\mathrm{H_2O}} + Y_{\mathrm{H_2}} + Y_{\mathrm{CO_2}} + Y_{\mathrm{CO}}$ [15].

E. Numerical methods

The governing equations are solved using an unstructured, fully-compressible finite-volume LES solver. As described by [16, 17], the Euler fluxes are spatially discretized using a sensor-based hybrid scheme, and a nominally fourth-order scheme is used for the viscous fluxes. For the full finite-rate chemistry simulation, time integration will be performed using a second-order operator splitting algorithm [18]. In the present case employing the FPV model, a third-order Runge-Kutta scheme is used.

V. Propellant Injection

As the propellants are injected, the momentum flux ratio between the methane and liquid oxygen causes the formation of a shear layer, which leads to breakup and atomization of the LOX stream. Primary breakup and atomization of the injected LOX will not be modeled explicitly; rather, the LOX stream is assumed to take the shape of a cone, and Lagrangian particles of LOX are injected along it, as described by Potier [19]. In the Eulerian phase, the cone is modeled as an adiabatic wall. A no-slip condition is applied to this wall because, as compared to a slip wall, the resulting velocity

profile better represents the effect of the large velocity gradient in the shear layer between the liquid and gas phases. The ratio of this cone's length to the initial stream diameter is determined using the correlation of Woodward [20]:

$$L/D_l = 0.0025 \left(\frac{\rho_g}{\rho_l}\right)^{-0.44} Re_l^{0.76} We_g^{-0.22} \tag{6}$$

where L and D_l are the length and base diameter of the cone, respectively, and ρ_g and ρ_l are the gas and liquid phase densities. Re_l is the liquid phase Reynolds number and We_g is the gas phase Weber number, respectively defined as:

$$Re_l = \frac{\rho_l u_l D_l}{\mu_l} \tag{7}$$

$$We_g = \frac{\rho_g (u_g - u_l)^2 D_l}{\sigma} \tag{8}$$

where μ_l is the liquid-phase kinematic viscosity, u_g is the gas-phase velocity, and σ is the surface tension. After accounting for the expansion of the methane flow as it enters the chamber, this yields a cone length of 10.27 mm in this case.

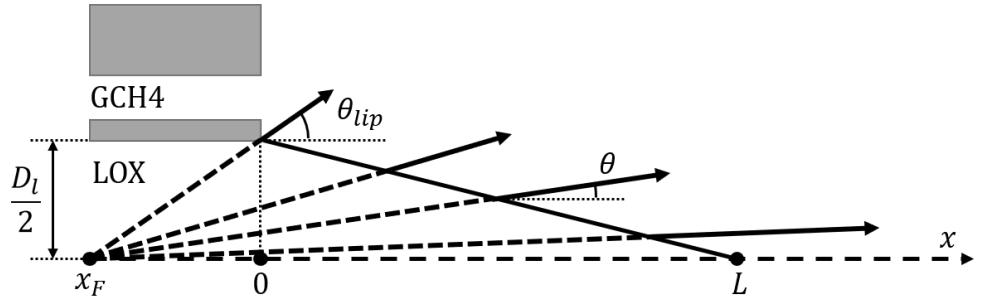

Fig. 1 LOX injection cone spray angle. (Adapted from [19].)

As depicted in Fig. 1, the spray is injected at an angle relative to the cone's axis, starting from a fixed θ_{lip} and decreasing to 0 at the tip of the cone. θ_{lip} is computed using the correlation of Hopfinger [21]:

$$\theta_{\text{lip}} = \frac{\pi}{4} - \tan^{-1}\left(\frac{\sqrt{J}}{12}\right) \tag{9}$$

where J is the momentum flux ratio of the propellants. This yields a value of 0.637 radians in this case. The angle θ varies along the length of the cone according to the following relationship from Potier [19]:

$$\tan(\theta) = \frac{D_l}{2(x - x_F)} \tag{10}$$

where x is the axial distance from the focal point position, x_F. This focal point position is computed as:

$$x_F = \frac{D_l/2}{\tan\left(\theta_{\text{lip}}\right)} \tag{11}$$

The diameter of the LOX droplets is assumed to follow a Rosin-Rammler distribution, and the parameters of this distribution are based on the work of Ramcke et al. [22] which modeled LOX flashing in the same Manfletti case. The minimum diameter is 10 μm, the maximum is 20 μm, and the mean is 16 μm.

VI. Ignition

The laser ignition process comprises plasma kernel creation, absorption of laser energy by the plasma kernel, and relaxation of the non-equilibrium plasma to an equilibrium state, thus releasing heat energy. Precise simulation of all processes involved in forming and developing the plasma kernel requires detailed consideration of plasma physics [23] and is beyond the scope of this work. Instead, in the final simulation, we will only model the long-time heat release by the plasma kernel to the surrounding flow field as a Gaussian energy deposition in time and space [6].

VII. Model Configuration

A fully block structured 3D mesh was developed for the RCS breadboard combustor, with the geometry simplified by the removal of the optical window regions on the side of the chamber. This mesh, comprised of approximately 1.8 million cells, is depicted in Fig. 2

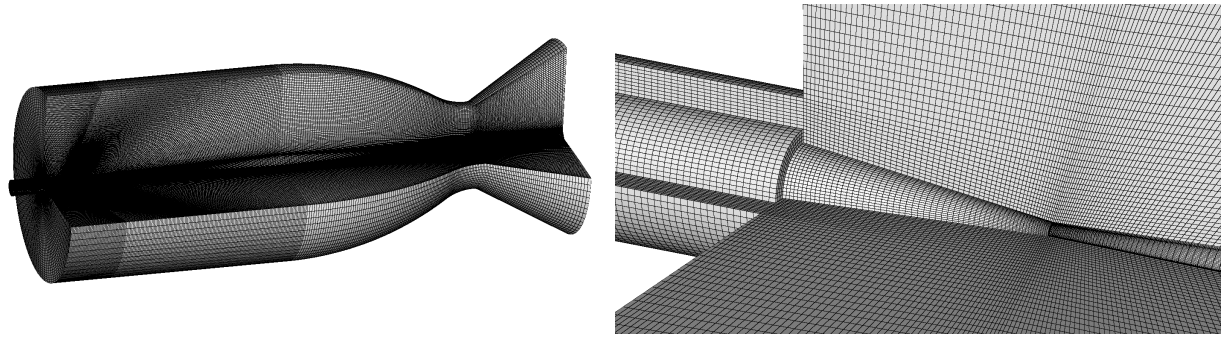

(a) Full mesh. **(b) Highlight of LOX cone.**

Fig. 2 Fully structured mesh of the RCS breadboard combustor with simplified geometry. The LOX cone has been removed from the mesh as described in Sec. V.

The boundary conditions for the simulation are depicted in Fig. 3. The chamber walls and the walls of the fuel injector are assumed adiabatic, with a no-slip condition. The outlet is a supersonic pressure outlet, and the fuel inlet is a subsonic mass flow inlet. As discussed in Sec. V, the LOX cone is modeled as an adiabatic, no-slip wall, along which the spray is injected. A parcel size of 1000 was used to reduce the computational cost of simulating the droplets by reducing the number of particles, while maintaining the proper evaporation rate of the individual droplets at the specified diameter.

In the present simulation, the domain was initialized as a stoichiometric mixture, with progress variable $C = 0.2$, with a corresponding temperature of 1162.2 K. The pressure was initialized to the nominal chamber pressure of the Manfletti case, 1.6 bar. By doing this, the simulation is effectively already ignited, allowing the flame to reliably develop over time. To allow time for this development,

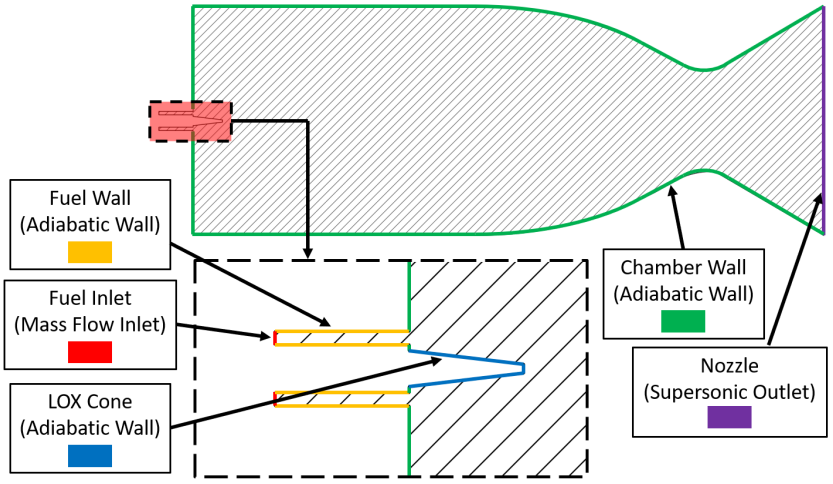

Fig. 3 Prescribed boundary conditions for the present simulation.

the present simulation was run for approximately 4.5 flow-through times (where a flow-through time based on volume replacement is approximately 8 ms).

VIII. Results

The results of the reacting simulation are depicted in Fig. 4. Several features are notable. Firstly, in the plot of mixture fraction, it is evident that the annular fuel stream is flared out away from the LOX cone as it enters the chamber. This behavior is caused by the LOX spray, which expands significantly as it evaporates. Correspondingly, there is a region of high O_2 concentration near the cone, as shown in Fig. 5. We can observe qualitatively similar behavior in the pre-ignition Schlieren imagery of the Manfletti case [5], where the flashing LOX spray expands significantly to form a wide, dense region of O_2.

In the plot of normalized progress variable, we may note that most of the combustor is filled with equilibrium products of combustion. In the majority of the combustor, the mixture fraction corresponding to a well-mixed composition also corresponds to near-equilibrium $\tilde{C}$ values. We may also note that there is a significant region of unburned mixture exiting the chamber through the nozzle, indicating that the flame is not yet fully developed at this time in the simulation.

In the plot of temperature, the low temperature of the reactants is clearly visible. Since the chamber walls were modeled as adiabatic, there is no thermal boundary layer present, indicated by the lack of temperature gradients normal to the walls. We may note that the region of unburned mixture exiting the chamber has been heated to combustion temperatures but has not yet had time to react.

Fig. 5 depicts the Lagrangian LOX spray in an isometric view. In this figure, we may note the large concentration of droplets located near the LOX cone, where they are injected. The droplets quickly evaporate, rapidly reducing in diameter as they are carried by the flow, and creating the region of high O_2 concentration. Eventually, shear-layer instabilities lead to mixing of the gaseous O_2 with the CH_4 stream, as is visible in the turbulent eddy structures.

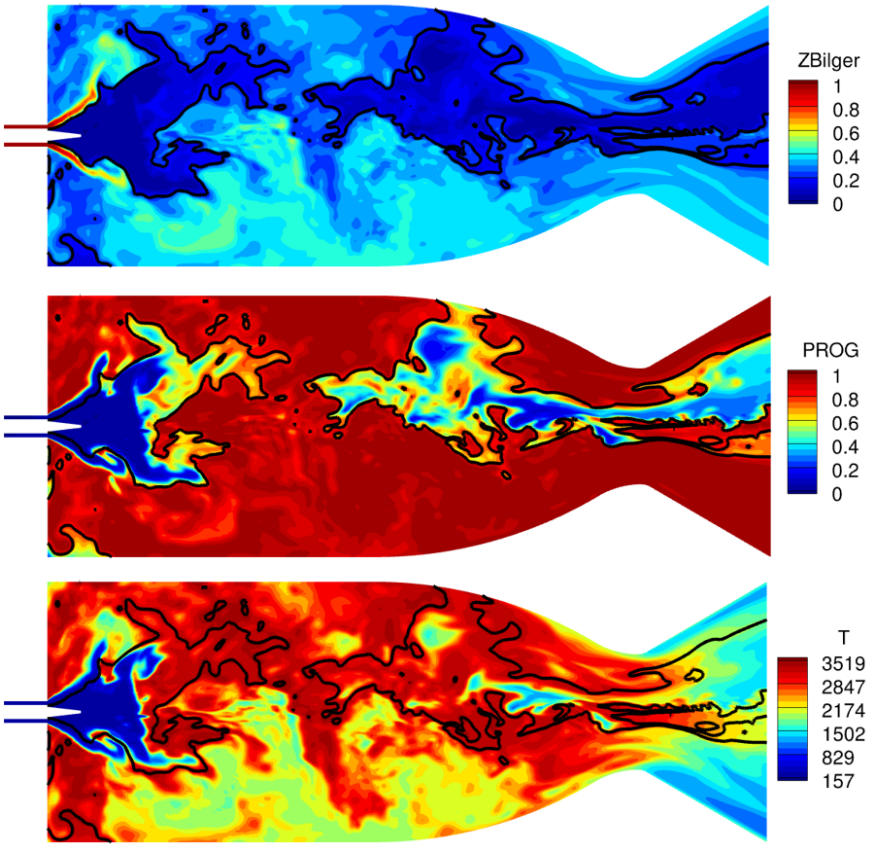

Fig. 4 Instantaneous contours of mixture fraction, normalized progress variable, and temperature are shown in a section of the combustor. The stoichiometric contour is highlighted in each with a bold black line.

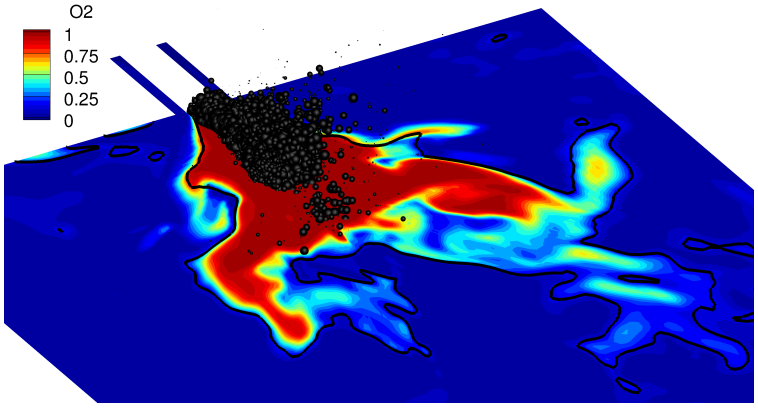

Fig. 5 A 3D, isometric view of the combustor is shown, with the LOX spray depicted as black spheres, each representing a parcel of 1000 droplets. The diameter of the spheres is proportional to the diameter of the droplets. Contours of O_2 mass fraction are also shown in a section, with the stoichiometric contour highlighted in black.

IX. Conclusion and Future Work

The present work has successfully demonstrated the application of the LSP model to LOX droplets in a reacting simulation of the RCS breadboard subscale rocket combustor at the DLR M3.1 test bench. The spray evaporated and burned as expected, and exhibited behavior that is qualitatively similar to the experimental results. This research has effectively laid the groundwork for a full simulation of ignition in this combustor. In the future, an ignition model will be implemented and verified. The flash evaporation model will also be implemented, and the entire ignition sequence will be simulated using finite rate chemistry. Mesh convergence analysis will be performed to verify that the solution is accurate. The final work will track the ignition process over time, following the flame through the four phases described by Schmidt et al. [24]: primary ignition, propagation, anchoring, and stabilization. It will compare these data to the experimental results of Manfletti, and provide information on quantities of engineering interest such as chamber pressure and wall heat flux.

Acknowledgments

This work is supported by NASA Award #NNX15AV04A and the Department of Energy through the Stanford PSAAP III Center, as well as the NASA Space Technology Graduate Research Opportunities program, grant number #80NSSC20K1171. Computational resources were provided by NASA High-End Computing (HEC) Program through NASA Advanced Supercomputing (NAS) Division at Ames Research Center.

References

[1] Lockheed Missiles and Space Company, "Propellant Selection for Spacecraft Propulsion Systems. Volume 1 - Results, Conclusions, and Recommendations," Tech. rep., NASA Office of Advanced Research and Technology, 1968.

[2] Muscatello, A., and Santiago-Maldonado, E., "Mars in situ resource utilization technology evaluation," *50th AIAA Aerospace Sciences Meeting Including the New Horizons Forum and Aerospace Exposition*, AIAA Paper 2012-360, 2012. doi:10.2514/6.2012-360.

[3] Vernin, H., and Pempie, P., "LOx/CH4 and LOx/LH2 heavy launch vehicle comparison," *45th AIAA/ASME/SAE/ASEE Joint Propulsion Conference & Exhibit*, AIAA Paper 2009-5133, 2009. doi:10.2514/6.2009-5133.

[4] Waxenegger, G., Riccius, J., Zametaev, E., Deeken, J., and Sand, J., "Implications of cycle variants, propellant combinations and operating regimes on fatigue life expectancies of liquid rocket engines," *7th European Conference for Aeronautics and Space Sciences, Milan, Italy*, 2017, pp. 3–6.

[5] Manfletti, C., "Laser ignition of an experimental cryogenic reaction and control thruster: pre-ignition conditions," *Journal of Propulsion and Power*, Vol. 30, No. 4, 2014, pp. 925–933. doi:10.2514/1.B34916.

[6] Lacaze, G., Cuenot, B., Poinsot, T., and Oschwald, M., "Large eddy simulation of laser ignition and compressible reacting flow in a rocket-like configuration," *Combustion and Flame*, Vol. 156, No. 6, 2009, pp. 1166–1180. doi:10.1016/j.combustflame.2009.01.004.

[7] Mohaddes, D., Xie, W., and Ihme, M., "Analysis of low-temperature chemistry in a turbulent swirling spray flame near lean blow-out," *Proceedings of the Combustion Institute (In Press)*, 2020. doi:10.1016/j.proci.2020.08.030.

[8] Vreman, A. W., "An eddy-viscosity subgrid-scale model for turbulent shear flow: Algebraic theory and applications," *Physics of Fluids*, Vol. 16, No. 10, 2004, pp. 3670–3681. doi:10.1063/1.1785131.

[9] Légier, J. P., Poinsot, T., Varoquié, B., Lacas, F., and Veynante, D., "Large eddy simulation of a non-premixed turbulent burner Using a dynamically thickened flame model," *IUTAM Symposium on Turbulent Mixing and Combustion*, Kluwer Academic Publishers, 2002, pp. 315–326. doi:10.1007/978-94-017-1998-8_27.

[10] Miller, R., Harstad, K., and Bellan, J., "Evaluation of equilibrium and non-equilibrium evaporation models for many-droplet gas-liquid flow simulations," *International Journal of Multiphase Flow*, Vol. 24, No. 6, 1998, pp. 1025–1055. doi:10.1016/S0301-9322(98)00028-7.

[11] Ranz, W., and Marshall, W., "Evaporation from drops, Part I," *Chemical Engineering Progress*, Vol. 48, No. 3, 1952.

[12] Smith, G. P., Golden, D. M., Frenklach, M., Moriarty, N. W., Eiteneer, B., Goldenberg, M., Bowman, C. T., Hanson, R. K., Song, S., Gardiner Jr, W., et al., "GRI-Mech 3.0, 1999," *URL http://www.me.berkeley.edu/gri_mech*, 2011.

[13] Ihme, M., Cha, C. M., and Pitsch, H., "Prediction of local extinction and re-ignition effects in non-premixed turbulent combustion using a flamelet/progress variable approach," *Proceedings of the Combustion Institute*, Vol. 30, No. 1, 2005, pp. 793–800. doi:10.1016/j.proci.2004.08.260.

[14] Pitsch, H., and Bollig, M., "Flamemaster, a computer code for homogeneous and one-dimensional laminar flame calculations," *Institut für Technische Mechanik, RWTH Aachen*, 1994.

[15] Ihme, M., Shunn, L., and Zhang, J., "Regularization of reaction progress variable for application to flamelet-based combustion models," *Journal of Computational Physics*, Vol. 231, No. 23, 2012, pp. 7715–7721. doi:10.1016/j.jcp.2012.06.029.

[16] Khalighi, Y., Nichols, J. W., Lele, S. K., Ham, F., and Moin, P., "Unstructured large eddy simulation for prediction of noise issued from turbulent jets in various configurations," *AIAA Paper 2011-2886*, 2011. doi:10.2514/6.2011-2886, URL http://arc.aiaa.org.

[17] Ma, P. C., Lv, Y., and Ihme, M., "An entropy-stable hybrid scheme for simulations of transcritical real-fluid flows," *Journal of Computational Physics*, Vol. 340, 2017, pp. 330–357. doi:10.1016/j.jcp.2017.03.022.

[18] Wu, H., Ma, P. C., and Ihme, M., "Efficient time-stepping techniques for simulating turbulent reactive flows with stiff chemistry," *Computer Phys. Comm.*, Vol. 243, 2019, pp. 81–96. doi:10.1016/J.CPC.2019.04.016.

[19] Potier, L., "Large Eddy Simulation of the combustion and heat transfer in sub-critical rocket engines," Ph.D. thesis, Institut National Polytechnique de Toulouse, May 2018.

[20] Woodward, R., Pal, S., Farhangi, S., and Santoro, R., "LOX/GH2 Shear Coaxial Injector Atomization Studies at Large Momentum Flux Ratios," *42nd AIAA/ASME/SAE/ASEE Joint Propulsion Conference and Exhibit*, American Institute of Aeronautics and Astronautics, Reston, Virigina, 2006. doi:10.2514/6.2006-5203.

[21] Hopfinger, E. J., "Atomisation d'un jet liquide par un jet de gaz coaxial : Un bilan des connaissances acquises," *Actes du Colloque Combustion dans les Moteurs Fusées*, 2001. URL https://hal.archives-ouvertes.fr/hal-00218187.

[22] Ramcke, T., Lampmann, A., and Pfitzner, M., "Simulations of injection of liquid oxygen/gaseous methane under flashing conditions," *Journal of Propulsion and Power*, 2018. doi:10.2514/1.B36412.

[23] Shneider, M. N., Zheltikov, A. M., and Miles, R. B., "Tailoring the air plasma with a double laser pulse," *Physics of Plasmas*, Vol. 18, No. 6, 2011. doi:10.1063/1.3601764.

[24] Schmidt, V., Klimenko, D., Haidn, O., Oschwald, M., Aurélie, N., Ordonneau, G., and Habbibalah, M., "Experimental investigation and modelling of the ignition transient of a coaxial H2/O2-injector," *5th International Symposium on Liquid Rocket Propulsion*, 2003.